J Radioanal Nucl Chem (2017) 311:917–927
DOI 10.1007/s10967-016-5098-5

Cyclic neutron activation analysis of large samples with a pulsed 14 MeV neutron source

Frank Mildenberger[1] · **Eric Mauerhofer**[1]

Received: 15 September 2016 / Published online: 8 November 2016

Abstract A method for the analysis of 200 L steel drums filled with various amounts of concrete and polyethylene by large sample cyclic neutron activation analysis (LS-CNAA) using a pulsed 14 MeV neutron source was developed. The elemental composition obtained for the homogenous samples was found to agree well with the expected values, the differences lying between −3 and +15%. For the heterogeneous samples, the results were found to agree with the expected values within ±39%. Depending on the polyethylene content of the samples, detection limits ranging between 14 and 24 mg kg^{-1} for cadmium, 520 and 740 mg kg^{-1} for mercury and 5.5 and 53 g kg^{-1} for lead were achieved for a counting time of about 30 min.

Keywords LS-CNAA · Concrete · Polyethylene · Thermal neutron die-away time

Introduction

The possibility to determine the element composition of large samples by neutron activation analysis at research reactors was reported first in 1993 by Bode and Overwater [1]. In the following years large sample instrumental neutron activation (LS-INAA) gained growing interest worldwide and various methods were developed and validated for the characterization of homogeneous and heterogeneous samples of kilogram size [2–10] or archeological items up to several liters in volume [11, 12]. Some specific works were dedicated to corrections for neutron absorption and gamma attenuation [13–15] and to the influence of inhomogeneities on the accuracy of LS-INAA [16]. It was also demonstrated that large objects may be investigated to some extent by prompt gamma neutron activation analysis (LS-PGNAA) using cold or thermal neutron beams [17–20]. However for the analysis of very large and thick items high energy neutrons such as emitted from isotopic sources (^{252}Cf, ^{241}Am–Be) or DD/DT neutron generators are of better choice due to their higher penetration depth compared to cold and thermal neutrons. Therefore NAA-systems using fast neutron sources were developed for various applications like explosive detection [21], industrial on-line bulk analysis [22] or waste characterization [23, 24]. It could be mentioned here the possibility to investigate also thick samples with the fission neutron beam of the research neutron source Heinz Maier-Leibnitz (FRM II, Garching) using the fast neutron gamma spectroscopy (FaNGaS) instrument [25, 26].

In this work large sample cyclic neutron activation analysis (LS-CNAA) of 200 L steel drums filled with concrete, polyethylene or a mix of concrete and polyethylene is carried out at the multi-element determination based on instrumental neutron activation (MEDINA) facility [24]. The drums are irradiated with pulsed 14 MeV neutrons and the prompt and delayed gamma-ray spectra recorded separately between the neutrons pulses. The methodology to determine the elemental composition of the large samples is presented. It includes the evaluation of the fast and thermal neutron flux using the steel drum as monitor and thermal neutron die-away times for correction of prompt gamma background interferences. The results are compared with those obtained for irradiation and

✉ Eric Mauerhofer
e.mauerhofer@fz-juelich.de

[1] Institute of Energy and Climate Research, Nuclear Waste Management and Reactor Safety, Forschungszentrum Jülich GmbH, 52425 Jülich, Germany

counting conditions preferably set for the acquisition of prompt gamma-ray spectra [27, 28]. The detection limits for the toxic elements cadmium, mercury and lead are evaluated.

Basic considerations

The timing diagram for the subsequent measurement of prompt and delayed gamma-rays between neutron pulses of length t_p is shown in Fig. 1. The prompt gamma-ray spectra are recorded over the time t_{pr} during the decrease of the thermal neutron flux and the delayed gamma-ray spectra over the time t_{dl} after disappearance of the thermal neutron flux. The repetition period is $T = t_p + t_{pr} + t_{dl}$. In a previous work [29] we showed that around 97% of the thermal neutrons have already vanished after a waiting time of about 12 ms from the end of the neutron pulse. The count rate $Z_{E\gamma}$ (s^{-1}) of a prompt gamma-ray measured during the time $t = n \times t_{pr}$, n being the number of neutron pulses, may be given by.

$$Z_{E\gamma} = \frac{m}{M} N \sigma_{E\gamma} \varepsilon_{E\gamma} \Phi_{\text{th,pr}} \tag{1}$$

where m (g) is the amount of element, M (g mol^{-1}) the molar mass of the element, N the Avogadro number, $\sigma_{E\gamma}$ (cm^2) the partial cross section for gamma-ray production [30, 31], $\varepsilon_{E\gamma}$ the gamma-ray detection efficiency and $\Phi_{\text{th,pr}}$ (cm^{-2} s^{-1}) the thermal neutron flux averaged within the sample over time t_{pr}. The contribution of epithermal neutrons is neglected here since the die-away time of thermal neutrons ($\sim$3 ms [29]) is much longer than the time required for thermalization of fast neutrons ($\sim$300 μs [32]).

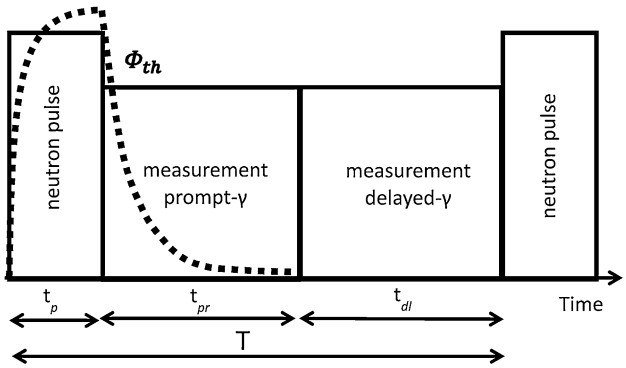

Fig. 1 Timing diagram for the cyclic neutron activation analysis of the large samples with a pulsed 14 MeV neutron source. t_p is the length of the neutron pulse, t_{pr} is the counting time for the measurement of prompt gamma rays, t_{dl} is the counting time for the measurement of delayed gamma rays and T is the repetition period. The *dot line* represents the behavior of the thermal neutron flux

For prompt gamma rays affected by background interferences a corrected count rate $Z'_{E\gamma}$ (s^{-1}) is calculated taking into account the difference in thermal neutron dynamics between irradiations with and without sample as.

$$Z'_{E\gamma} = Z_{E\gamma} - \frac{\Lambda_{E\gamma}}{\Lambda_{E\gamma,0}} Z_{E\gamma,0} \tag{2}$$

where $Z_{E\gamma,0}$ (s^{-1}) is the gamma-ray count rate measured without sample (empty drum) and $\Lambda_{E\gamma}$ (s) and $\Lambda_{E\gamma,0}$ (s) are the thermal neutron die-away-times determined from the count rate decay of the considered prompt gamma ray in irradiations with and without sample, respectively.

For delayed gamma rays of activation products, the cumulated count $P_{E\gamma}$ recorded may be expressed from the basic equation for cyclic activation [33] using the irradiation and counting parameters of timing diagram in Fig. 1. In the case of fast neutron activation it is given by

$$P_{E\gamma} = \frac{m}{M} N \theta \sigma_f \Phi_f \varepsilon_{E\gamma} I_{E\gamma} \left(1 - e^{-\lambda t_p}\right)\left(e^{-\lambda t_{pr}}\right)\left(1 - e^{-\lambda t_{dl}}\right) g(\lambda, T, n) \tag{3}$$

with

$$g(\lambda, T, n) = \frac{1}{\lambda}\left[\frac{n}{\left(1 - e^{-\lambda T}\right)} - \frac{e^{-\lambda T}\left(1 - e^{-n\lambda T}\right)}{\left(1 - e^{-\lambda T}\right)^2}\right] \tag{4}$$

where θ is the isotopic abundance, σ_f (cm^2) the isotopic absorption cross section for the considered fast (14 MeV) neutron reaction [34, 35], λ (s^{-1}) the decay constant of the formed activation product [36] and $I_{E\gamma}$ the intensity of the delayed gamma ray [36]. The average fast neutron flux Φ_f (cm^{-2} s^{-1}) during the neutron pulse may be expressed by [37].

$$\Phi_f = \Phi_{f,d} e^{-\Sigma d} \tag{5}$$

where $\Phi_{f,d}$ (cm^{-2} s^{-1}) is the average fast neutron flux at the drum surface and $d = 56$ cm the diameter of the steel drum. The total macroscopic cross section for 14 MeV neutrons Σ is calculated from the sample composition and using the microscopic cross section data given in [34].

In the case of thermal neutron activation and considering also the buildup of the thermal and epithermal neutron flux during the fast neutron pulse $P_{E\gamma}$ may be expressed by

$$P_{E\gamma} = \frac{m}{M} N h \sigma_{\text{th}} \varepsilon_{E\gamma} I_{E\gamma} \left(1 - e^{-\lambda t_{dl}}\right)\left(e^{-\lambda t_{pr}}\right)\left[\Phi_{\text{th,pr}}\left(1 - e^{-\lambda t_{pr}}\right) + \Phi_{\text{th,p}}\left[1 + (0.44 + I/\sigma_{\text{th}})F\right]\left(1 - e^{-\lambda t_p}\right)\right] g(\lambda, T, n) \tag{6}$$

with σ_{th} (cm^2) the isotopic thermal neutron capture cross section [35, 38, 39], I (cm^2) the isotopic resonance integral [35, 38, 39], and $F = 0.18 \pm 0.02$ [27] the epithermal to thermal neutron flux ratio. The average thermal neutron flux $\Phi_{\text{th,p}}$ (cm^{-2} s^{-1}) during the neutron pulse is related to

the average thermal neutron flux $\Phi_{th,pr}$ (cm^{-2} s^{-1}) determined after the pulse as

$$\Phi_{th,p} = \frac{\Phi_{th,pr}}{\left(1 - e^{-t_{pr}/\overline{\Lambda}}\right)} \left[\frac{t_{pr}}{\overline{\Lambda}\left(1 - e^{-t_p/\overline{\Lambda}}\right)} - \frac{t_{pr}}{t_p}\right] \quad (7)$$

where $\overline{\Lambda}$ (s) is the die-away time of thermal neutrons in the steel drum used for neutron flux monitoring [27].

The numerical determination of the gamma-ray detection efficiency $\varepsilon_{E\gamma}$ for the sample and the steel drum is well described in [27, 28]. It is based on a point source efficiency measurement and the application of a transfer function taking into account the sample and steel drum geometry, the gamma-ray attenuation and the apparent density of the sample.

Measurements

Homogeneous large samples consist of 200 L steel drums filled either with 76 concrete or polyethylene cylindrical bodies of same size (height: 20 cm, diameter 11 cm). The weights of the concrete and polyethylene blocks are 2.6 and 1.6 kg, respectively. The elemental composition of concrete is given in [24] and listed in the last column of Table 3 for the elements detected in this work. The weight concentration of hydrogen in polyethylene is 13 ± 1%. Inhomogeneous large samples consist of a mix of concrete and polyethylene blocks whose arrangements in the drums are described in detail in a previous PGNAA work [28]. Some relevant characteristics of the samples are given in Table 1.

LS-CNAA is performed at the MEDINA facility with a 14 MeV neutron generator operated in pulse mode at a neutron emission of 7.18 ± 0.93 × 10^7 s^{-1} for irradiation and an HPGe (104% relative efficiency) for prompt and delayed gamma rays measurement. The length of the neutron pulses is set to 2 ms and the repetition time to 40 ms. Using two multi channel analyzers the prompt gamma rays are detected after the neutron pulses for 18 ms and the delayed gamma rays for 20 ms directly after the prompt gamma-ray acquisition. Prompt and delay gamma-ray spectra are recorded for total counting time of 1620 and 1800 s, respectively. For background correction spectra of the empty drum are also recorded under the same condition as the samples. As an example, the prompt and delayed gamma-ray spectra recorded for the 200 L drum filled with concrete and the delayed gamma-ray spectrum recorded for the empty drum are shown together for various energy ranges in Figs. 2 and 3. The origin of the prompt and delayed gamma rays observed in the prompt gamma-ray spectra of the empty drum and the drum filled with concrete is well discussed in a previous work [27]. The delayed gamma rays of ^{71m}Ge ($T_{½}$ = 20.4 ms), ^{75m}Ge ($T_{½}$ = 47.7 s), ^{24m}Na ($T_{½}$ = 20.2 ms), ^{16}N ($T_{½}$ = 7.13 ms), ^{28}Al ($T_{½}$ = 2.24 m), ^{27}Mg ($T_{½}$ = 9.46 m) and ^{116m}In ($T_{½}$ = 53.4 m) already observed in the prompt gamma ray spectra are detected with a better counting statistics in the delayed gamma-ray spectra due to the absence of prompt gamma activity reducing thus the Compton background. Moreover the delayed gamma rays of the short and medium lived activation products ^{19}O ($T_{½}$ = 26.9 s), ^{20}F ($T_{½}$ = 11 s), ^{24}Na ($T_{½}$ = 14.95 h), ^{49}Ca ($T_{½}$ = 8.72 m), ^{52}V ($T_{½}$ = 3.74 m) and ^{56}Mn ($T_{½}$ = 2.56 h) are clearly identified. The isotope ^{19}O is produced mainly through (n,p)-reaction from the interaction of fast neutrons

Table 1 Thermal neutron die-away times Λ_{1_H}, Λ_{10_B} and $\Lambda_{28_{Si}}$ determined from the count rates of the prompt gamma rays at 2223, 477 and 3539 keV, respectively and mean thermal neutron die-away time in the steel drum $\overline{\Lambda}$ determined from the count rates of the ^{56}Fe prompt gamma rays at 352, 691 and 7361 keV

Sample	m_c (kg)	m_p (kg)	ρ_a (g cm^{-3})	Λ_{1_H} (ms)	Λ_{10_B} (ms)	$\Lambda_{28_{Si}}$ (ms)	$\overline{\Lambda}$ (ms)
Empty drum				2.59 ± 0.11	3.56 ± 0.25	2.71 ± 0.01	3.31 ± 0.07
HP	0	120.8	0.61	2.32 ± 0.07	2.72 ± 0.19	–	2.42 ± 0.05
HC	194.6	0	0.99	2.34 ± 0.05	2.37 ± 0.04	2.00 ± 0.02	2.32 ± 0.01
Ra1	184.3	6.4	0.97	2.25 ± 0.13	2.21 ± 0.01	1.95 ± 0.02	2.37 ± 0.01
Ra2	133.1	38.2	0.87	2.49 ± 0.08	2.12 ± 0.04	2.31 ± 0.03	2.33 ± 0.04
Ra3	71.7	76.3	0.75	2.27 ± 0.09	1.99 ± 0.04	2.05 ± 0.05	2.33 ± 0.05
Ra4	10.2	114.5	0.63	2.41 ± 0.11	2.03 ± 0.07	1.80 ± 0.05	2.24 ± 0.04
Ra5	61.4	82.7	0.72	2.48 ± 0.18	1.97 ± 0.02	2.11 ± 0.03	2.26 ± 0.02
Ra6	122.9	44.5	0.84	2.32 ± 0.17	1.98 ± 0.03	2.11 ± 0.05	2.33 ± 0.02
Ax1	145.9	30.2	0.89	2.29 ± 0.11	1.81 ± 0.07	1.91 ± 0.04	2.36 ± 0.03
Ax2	145.9	30.2	0.89	2.32 ± 0.13	1.90 ± 0.07	1.99 ± 0.04	2.34 ± 0.03
Ax3	97.3	60.4	0.80	2.46 ± 0.10	1.97 ± 0.02	2.14 ± 0.04	2.35 ± 0.03
Ax4	48.6	90.6	0.71	2.26 ± 0.09	1.84 ± 0.07	2.01 ± 0.04	2.36 ± 0.04

The weights of concrete and polyethylene are m_c and m_p, respectively and ρ_a is the apparent density. *HP* drum filled with polyethylene, *HC* drum filled with concrete. For heterogeneous samples the radial (Ra) and axial (Ax) arrangements of the concrete and polyethylene blocks in the drums are described in [28]

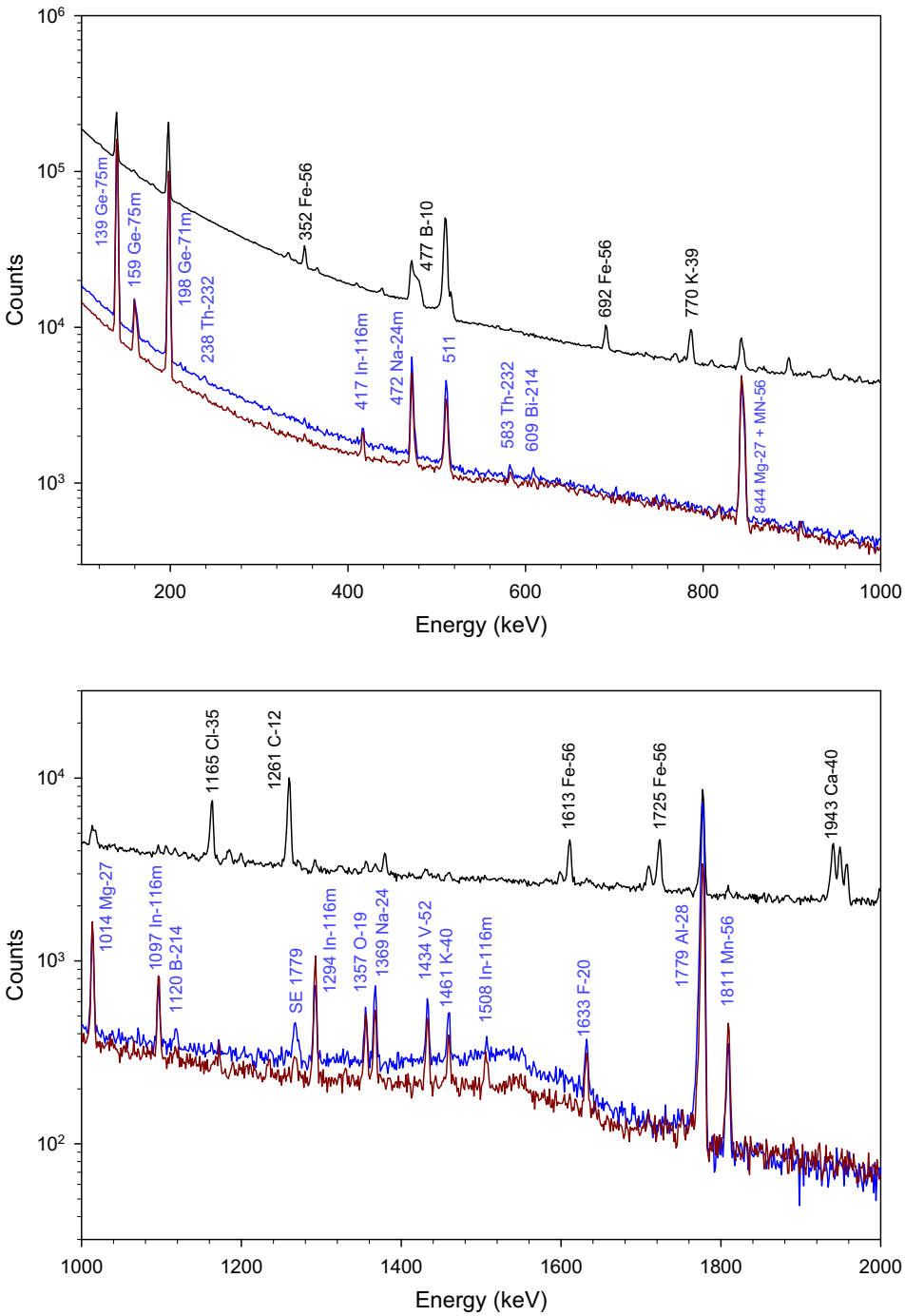

Fig. 2 Prompt (*black*) and delayed (*blue*) gamma-ray spectra in the energy range 100–2000 keV for the 200 L drum filled with concrete and delayed gamma-ray spectrum for the empty drum (*red*). (Color figure online)

with fluorine in the ^{6}LiF detector shielding. The formation of this isotope through thermal neutron capture of oxygen in concrete is negligible because of the low abundance of ^{18}O (0.205%) and the low neutron absorption cross section ($\sigma_{th} = 1.6 \times 10^{-4}$ b [35]). Consequently the oxygen content of concrete is determined via the fast neutron reaction ^{16}O(n,p)^{16}N ($\sigma_f = 0.042$ b [34]). The isotope ^{20}F is induced by epithermal/fast neutron capture of fluorine in the ^{6}LiF detector shielding as well as through the fast neutron reaction ^{23}Na(n,α)^{20}F ($\sigma_f = 0.140$ b [34]) from sodium in concrete. The isotope ^{24m}Na and ^{24}Na are induced through (n,α)-reaction from the interaction of fast neutrons with aluminum in the HPGe-detector housing and in concrete as well as through thermal/epithermal neutron capture of sodium in concrete. The cross section for the reaction ^{27}Al(n,α)^{24m}Na is $\sigma_f = 0.065$ b [35]. For the reaction ^{23}Na(n,γ)^{24m}Na the cross sections are $\sigma_{th} = 0.40$ b [35] and $I = 0.312$ b [38]. The isotope ^{49}Ca is produced by thermal/epithermal neutron capture of calcium in concrete, ^{48}Ca(n,γ)^{49}Ca ($\sigma_{th} = 1.09$ b [38], $I = 0.485$ b [38]) The isotope ^{28}Al is produced by thermal/epithermal neutron

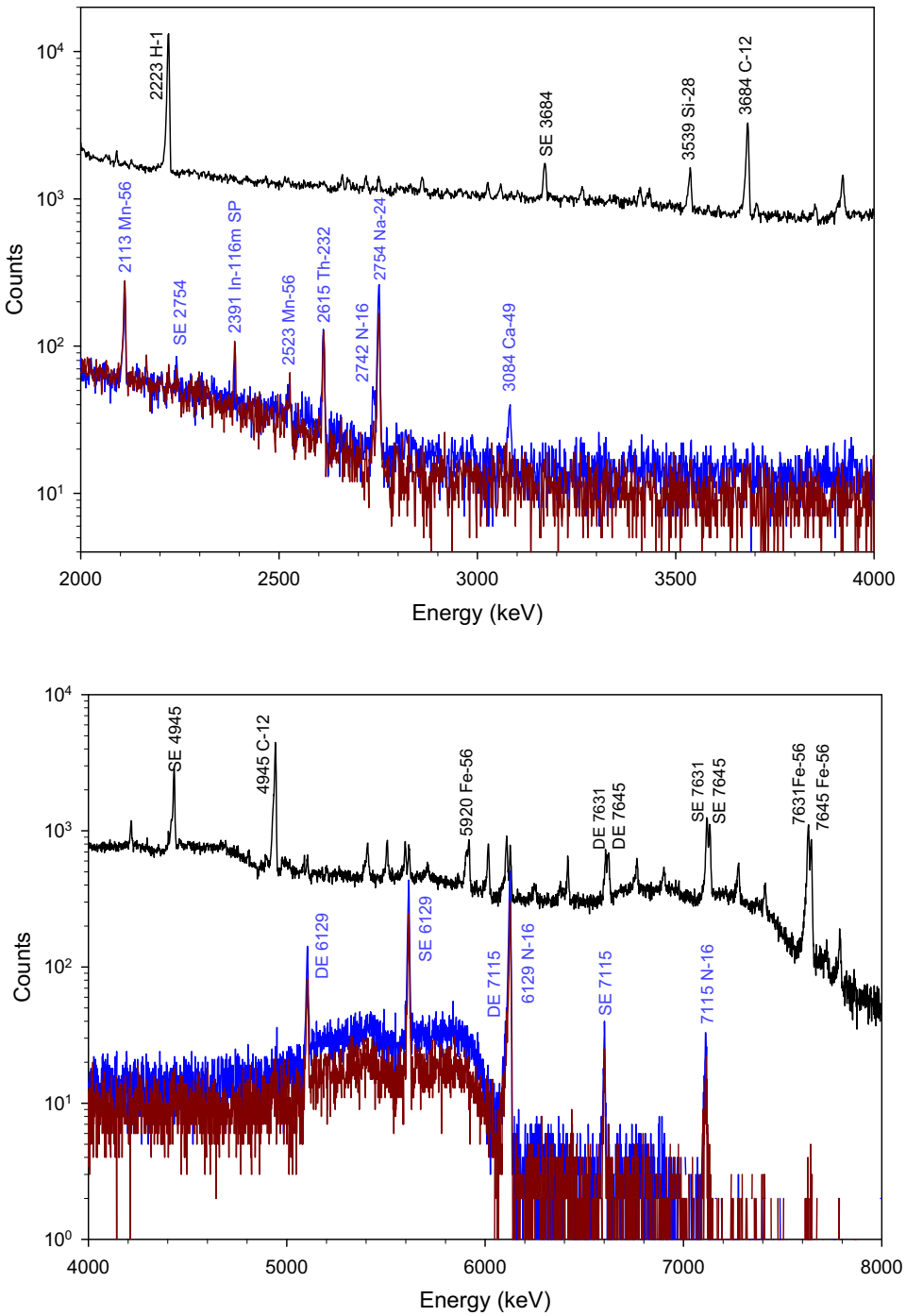

Fig. 3 Prompt (*black*) and delayed (*blue*) gamma-ray spectra in the energy range 4000–8000 keV for the 200 L drum filled with concrete and delayed gamma-ray spectrum for the empty drum (*red*). (Color figure online)

capture of aluminum in concrete, ^{27}Al(n,γ)^{28}Al ($\sigma_{th} = 0.230$ b [38], $I = 0.123$ b [38]) as well as by the reaction ^{28}Si(n,p)^{28}Al ($\sigma_f = 0.279$ b [34]) from interaction of fast neutron with silicon in concrete. The isotope ^{56}Mn is generated through the reaction ^{56}Fe(n,p)^{56}Mn ($\sigma_f = 0.115$ b [34]) from interaction of fast neutrons with the steel drum. The isotope ^{52}V is supposed to be produced by (n,p)-reaction from the interaction of fast neutrons with chromium contained in the steel housing of the neutron generator. Another possible source of production for ^{52}V could be the thermal neutron capture of vanadium traces in graphite [24].

Knowledge on the die-away time of thermal neutrons is required to correct the count rate of prompt gamma rays suffering from background interferences (Eq. 2) as well as to calculate the mean thermal neutron flux built during the fast neutron pulses (Eq. 7). Die-away times were determined in a previous work [29] for the empty drum and the drum filled either with concrete or polyethylene recording

prompt gamma-ray spectra at various waiting times after the end of the fast neutron pulses and analyzing the decay of the count rate of selected prompt gamma-rays. The same method is applied here to ascertain the die-away times for the drums filled with mixtures of concrete and polyethylene focusing on the background interfering prompt gamma rays of ^{1}H (2223.2 keV), ^{10}B (477.6 keV), and ^{28}Si (3538.9 keV) and the prompt gamma-rays of ^{56}Fe (352.3, 691.9, 7631.5 keV) emitted from the steel drum. The resulting die-away times are presented in Table 1. The values obtained for the various samples are comparable indicating that the neutron dynamics is mainly governed by the large amount of graphite composing the irradiation chamber. However, in comparison to the values deduced for the empty drum, the presence of sample in the drum induces a reduction of the die-away time by 8–43% according to the considered gamma-ray i.e. isotope.

The steel drum is used to monitor the thermal and fast neutron flux within the sample which values are given in Table 2. The thermal neutron flux after the neutron pulses $\Phi_{\text{th,pr}}$ is determined from the count rates of the iron prompt gamma rays by means of relation (1). The thermal neutron flux during the neutron pulses $\Phi_{\text{th,p}}$ is calculated from $\Phi_{\text{th,pr}}$ by means of relation (7) using the die-away time of thermal neutrons in the steel drum ($\overline{A}$-value given in Table 1). The fast neutron flux at the steel drum surface $\Phi_{f,d}$ is estimated from the 1811 keV gamma ray of ^{56}Mn using Eq. (4). The fast neutron flux within the sample Φ_f is calculated by means of relation (5) with a Σ-value (Table 2) based on the known sample composition and the apparent density of the sample ρ_a (Table 1). As expected the fast neutron flux decreases exponentially with increasing polyethylene content i.e. hydrogen weight concentration, while the thermal neutron flux (during and between the pulses) decreases smoothly. For the later the deviation between lowest (drum filled with concrete) and highest (drum filled with polyethylene) value is 36 ± 5%. This deviation is higher than this obtained in the PGNAA of the same samples (14 ± 1%) [28], due to different irradiation and counting conditions (t_p = 2 ms, T = 40 ms and t_{pr} = 18 ms in this work, t_p = 50 μs, T = 1 ms and t_{pr} = 930 μs in [28]). As shown in Fig. 4 the thermal to fast neutron flux ratio during the neutron pulses increases asymptotically according to the polyethylene content of the sample reflecting the competition between the moderation of fast neutrons and the absorption of thermal neutrons by hydrogen.

Results

The elemental composition of concrete determined by LS-CNAA is given in Table 3. The weight concentrations agree well with the values obtained by PGNAA of small samples at the Budapest Research Reactor [24] and by PGNAA of the massive concrete sample [27] taking into account the respective uncertainties. The good agreement obtained for hydrogen, boron and silicon using their prompt gamma-rays confirms the validity of the corrections for background interferences using the die-away time of

Table 2 Average thermal neutron fluxes $\Phi_{\text{th,pr}}$ and $\Phi_{\text{th,p}}$ within the sample after and during the neutron pulses, respectively

Sample	PE (%)	Σ (cm^{-1})	$\Phi_{\text{th,pr}} \times 10^{-3}$ (cm^{-2} s^{-1})	$\Phi_{\text{th,p}} \times 10^{-3}$ (cm^{-2} s^{-1})	$\Phi_{f,d} \times 10^{-3}$ (cm^{-2} s^{-1})	$\Phi_f \times 10^{-3}$ (cm^{-2} s^{-1})	Σ_{exp} (cm^{-1})	$\Phi_{f\,\text{exp}} \times 10^{-3}$ (cm^{-2} s^{-1})
ED	–	–	1.8 ± 0.3	5.5 ± 0.9	135 ± 6	–	–	–
HP	100	0.0689	0.9 ± 0.1	3.9 ± 0.6	63 ± 4	1.33 ± 0.08	0.069	1.3 ± 0.4
HC	0	0.0392	1.4 ± 0.2	6.2 ± 0.9	133 ± 6	14.8 ± 0.7	0.038	15.4 ± 1.2
Ra1	3.4	0.0422	1.3 ± 0.2	5.6 ± 0.9	65 ± 3	6.1 ± 0.5	0.046	4.9 ± 0.5
Ra2	22.3	0.0464	1.2 ± 0.2	5.3 ± 0.9	58 ± 4	4.3 ± 0.3	0.048	3.9 ± 0.5
Ra3	51.6	0.0569	1.1 ± 0.2	4.8 ± 0.9	35 ± 3	1.4 ± 0.1	0.060	1.2 ± 0.2
Ra4	91.8	0.0672	1.0 ± 0.2	4.6 ± 0.9	49 ± 3	1.14 ± 0.07	0.065	1.3 ± 0.2
Ra5	57.4	0.0578	1.1 ± 0.2	5.0 ± 0.9	54 ± 4	2.1 ± 0.2	0.056	2.3 ± 0.3
Ra6	26.6	0.0476	1.1 ± 0.2	4.9 ± 0.9	47 ± 3	3.3 ± 0.3	0.050	2.9 ± 0.3
Ax1	17.1	0.0440	1.3 ± 0.2	5.7 ± 0.9	65 ± 5	5.6 ± 0.4	0.046	4.9 ± 0.7
Ax2	17.1	0.0440	1.2 ± 0.2	5.3 ± 0.9	62 ± 4	5.3 ± 0.4	0.047	4.5 ± 0.5
Ax3	38.3	0.0525	1.1 ± 0.2	4.8 ± 0.9	62 ± 4	3.3 ± 0.2	0.053	3.2 ± 0.3
Ax4	65.1	0.0612	1.0 ± 0.2	4.3 ± 0.9	48 ± 3	1.6 ± 0.2	0.066	1.2 ± 0.1

Average fast neutron flux $\Phi_{f,d}$ at the steel drum surface. Average fast neutron flux Φ_f within the sample determined with the total macroscopic cross section for 14 MeV neutrons Σ based on a known sample composition. Average fast neutron flux $\Phi_{f\,\text{exp}}$ within the sample determined with the total macroscopic cross section for 14 MeV neutrons Σ_{exp} based on the PGNAA analytical results (see text)

thermal neutrons. For aluminum, silicon and calcium, the weight concentrations deduced from the delayed gamma rays of the activation products are in accord with those obtained from the prompt gamma measurements. In the case of aluminum and silicon whose weight concentrations are determined from fast neutron reactions [(n,α) and (n,p)] the contributions of interfering thermal neutron reactions $^{23}Na(n,\gamma)^{24m}Na$ and $^{27}Al(n,\gamma)^{28}Al$ are calculated by means of Eq. (6). The sodium weight concentration is deduced from the $^{23}Na(n,\alpha)^{20}F$ reaction and the aluminum weight concentration from the prompt gamma-rays measurement. The oxygen weight concentration agrees well with the value estimated supposing the maximal oxidation state for all elements. In the case of the drum filled with polyethylene the weight concentration of hydrogen (13 ± 2%) agrees well with the expected value (13 ± 1%).

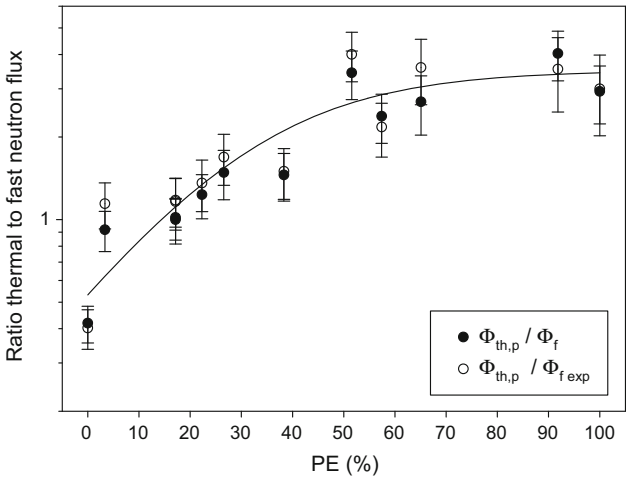

Fig. 4 Ratio thermal to fast neutron flux in the neutron pulses as a function of the polyethylene content of the sample

The ratios of measured to expected amounts of the considered elements in the samples composed of concrete and polyethylene are given in Table 4. For some samples no net signal for the delayed gamma rays is observed owing to a low fast neutron flux, a low concrete content and/or an unfavorable arrangement of the concrete blocks relative to the polyethylene blocks. The deviations between measured and expected values are ranging between −31

Table 3 Elemental composition of concrete determined in this work (LS-CNAA) compared to the LS-PGNAA performed at the MEDINA facility [27] and to the PGNAA of small samples performed at the Budapest research reactor [24, 40]

Element/isotope	$E\gamma$ (keV)	LS-CNAA	LS-PGNAA	PGNAA small sample
H/^{1}H	2223.2	1.35 ± 0.27%	1.24 ± 0.11%	1.40 ± 0.07%
B/^{10}B	447.6	92 ± 22 ppm	99 ± 9 ppm	95 ± 2 ppm
O/$^{16}O(n,p)^{16}N$	6128.6	48.5 ± 4.7%		
	7115.2	48.3 ± 4.8%		
		48.4 ± 0.1%[a]	49.3 ± 1.0%[b]	47.3 ± 2.5%[b]
Na/^{24}Na	869.2			0.52 ± 0.11%
Na/$^{23}Na(n,\alpha)^{20}F$	1633.6	0.59 ± 0.09%		
Al/^{27}Al	7724.0	5.0 ± 1.1%	5.1 ± 1.1%	4.9 ± 0.1%
Al/$^{27}Al(n,\alpha)^{24m}Na$	472.2	4.7 ± 0.9%		
		4.9 ± 0.2%[a]		
Si/^{28}Si	1273.3	18.8 ± 4.2%	18.5 ± 4.0%	
	2092.9	16.1 ± 3.8%	17.4 ± 4.3%	
	3538.9	17.1 ± 4.1%	17.7 ± 2.8%	
Si/$^{28}Si(n,p)^{28}Al$	1778.9	22.5 ± 4.8%		
		18.6 ± 2.8%[a]	17.9 ± 0.6%[a]	17.4 ± 0.2%
K/^{39}K	770.3	1.4 ± 0.3%	1.23 ± 0.19%	1.38 ± 0.06%
Ca/^{40}Ca	1942.7	22.4 ± 3.9%	21.4 ± 2.2%	
	2001.3	21.0 ± 4.2%	23.6 ± 2.6%	
	2009.8	22.5 ± 4.6%	23.6 ± 3.1%	
	4418.5	23.7 ± 4.3%	21.8 ± 2.8%	
	6419.6	22.4 ± 4.1%	22.9 ± 3.5%	
Ca/$^{48}Ca(n,\gamma)^{49}Ca$	3084.0	22.1 ± 4.6%		
		22.3 ± 0.8%[a]	22.7 ± 1.0%[a]	23.3 ± 0.6%
Ti/^{48}Ti	1381.7	0.30 ± 0.07%	0.25 ± 0.03%	0.26 ± 0.06%

[a] Arithmetic mean

[b] Estimated supposing the maximum oxidation state for all elements detected

and 41% essentially due to the simplification of the quantification model where the drum is assumed to be filled with a concrete matrix of apparent density ρ_a. The deviations are comparable than these obtained in the PGNAA of the samples (−27 to 58%) [28]. The spread of the data, including those of the homogenous samples (only concrete or polyethylene) is represented by box-and-whisker plots in Fig. 5. In the majority of cases the amount of hydrogen and oxygen is underestimated. Only 14% of all data are identified as outliers. The Gaussian fit of all data (see Fig. 5) provides a median $\mu = 0.98 \pm 0.01$ and a standard deviation $\sigma = 0.19 \pm 0.01$. Thus the elements amounts in the heterogeneous samples made of concrete and polyethylene may be determined with a conservative uncertainty of 39% (2σ), a value comparable to this achieved by PGNAA (34%) [28].

A critical point related to the quantification with fast neutron reactions is the knowledge of the total macroscopic cross section Σ to calculate the flux of fast neutrons within the sample. As mentioned above it was determined from the known sample composition though it may be estimated after some considerations from the results obtained by thermal neutron capture. A net signal of the oxygen delayed gamma ray correlates to a high fast neutron flux indicating the sample being composed mainly by concrete (samples HC, Ra1, Ra2, Ra6, Ax1 and Ax2). If oxygen is not detected, the polyethylene content is calculated from the hydrogen prompt gamma-ray and the difference to the sample mass is associated to concrete (samples HP, Ra3, Ra4, Ra5, Ax3 and Ax4). The macroscopic cross sections Σ_{exp} obtained in this way and the resulting fast neutron fluxes Φ_{fexp} agree well with the corresponding data deduced from the known sample composition (see Table 2; Fig. 4). Hence, quantification of the elements detected via fast neutron reactions based on Φ_{fexp} agree well with the results obtained from a priori knowledge of sample composition within a margin of $12 \pm 9\%$.

The limits of detection (3σ of background signal) are calculated for the toxic elements cadmium, mercury and lead in the samples. For cadmium and mercury it is calculated by means of relation (1) using the prompt gamma rays at 558.3 keV ($\sigma_{E\gamma} = 1860$ b) and 1693.3 keV ($\sigma_{E\gamma} = 56$ b), respectively. The detection limit for lead is calculated by means of relation (3) using the delayed gamma ray at 1063.7 keV of ^{207m}Pb ($T_{1/2} = 805$ ms) induced through the fast neutron reaction ^{208}Pb(n,2n)^{207m}Pb ($\sigma_f = 1.63$ b [35]) For the concrete sample, the detection limits are 14 and 520 mg kg^{-1} for cadmium and mercury, respectively for an assay of 1620 s and 5.5 g kg^{-1} for lead for an assay of 1800 s. The values obtained for cadmium and mercury are about 3.5 higher than the detection limits determined for an

Table 4 Ratios of the measured to excepted amounts for the elements detected in the mixed samples composed of concrete and polyethylene

Sample	H (p)	B (p)	O (d)	Na (d)	Al (p)	Al (d)	Si (p)	Si (d)	K (p)	Ca (p)	Ca (d)	Ti (p)
Ra1	0.93 ± 0.23	0.75 ± 0.25	0.82 ± 0.08	1.04 ± 0.27	1.01 ± 0.25	1.15 ± 0.09	0.84 ± 0.04	1.37 ± 0.14	0.95 ± 0.16	0.87 ± 0.07	0.80 ± 0.21	1.09 ± 0.32
Ra2	0.86 ± 0.21	0.84 ± 0.21	0.83 ± 0.06	0.97 ± 0.28	1.21 ± 0.26	1.35 ± 0.11	0.70 ± 0.05	1.50 ± 0.19	1.06 ± 0.17	1.05 ± 0.06	0.94 ± 0.20	1.23 ± 0.35
Ra3	0.91 ± 0.20	0.77 ± 0.23	–	–	1.36 ± 0.28	–	0.82 ± 0.04	–	1.02 ± 0.16	0.98 ± 0.06	–	1.01 ± 0.30
Ra4	1.01 ± 0.21	1.09 ± 0.25	–	–	–	–	0.97 ± 0.04	–	1.03 ± 0.16	1.20 ± 0.08	–	1.09 ± 0.31
Ra5	0.82 ± 0.21	1.17 ± 0.23	–	–	–	–	1.16 ± 0.04	–	1.38 ± 0.21	1.08 ± 0.07	–	1.26 ± 0.36
Ra6	0.77 ± 0.22	1.00 ± 0.22	1.12 ± 0.19-	1.20 ± 0.28	1.13 ± 0.26	1.29 ± 0.10	1.02 ± 0.03	1.38 ± 0.14	0.85 ± 0.24	1.11 ± 0.07	0.97 ± 0.22	1.13 ± 0.32
Ax1	0.83 ± 0.21	0.69 ± 0.23	0.94 ± 0.07	–	0.88 ± 0.30	0.75 ± 0.08	0.76 ± 0.05	1.19 ± 0.12	1.03 ± 0.17	0.88 ± 0.07	0.81 ± 0.23	0.87 ± 0.30
Ax2	0.85 ± 0.21	0.75 ± 0.20	0.94 ± 0.06	–	1.15 ± 0.27	0.88 ± 0.09	0.78 ± 0.04	1.44 ± 0.16	0.96 ± 0.16	0.91 ± 0.06	0.84 ± 0.22	0.83 ± 0.30
Ax3	0.91 ± 0.22	1.37 ± 0.28	–	–	1.12 ± 0.26	–	0.99 ± 0.03	1.42 ± 0.14	1.22 ± 0.17	1.27 ± 0.08	0.98 ± 0.22	1.13 ± 0.34
Ax4	0.98 ± 0.22	1.41 ± 0.29	–	–	0.88 ± 0.31	–	0.95 ± 0.03	1.51 ± 0.18	1.09 ± 0.17	1.26 ± 0.08	–	0.69 ± 0.30

Determination through prompt gamma rays (p) and through delayed gamma-rays (d) as given in Table 3

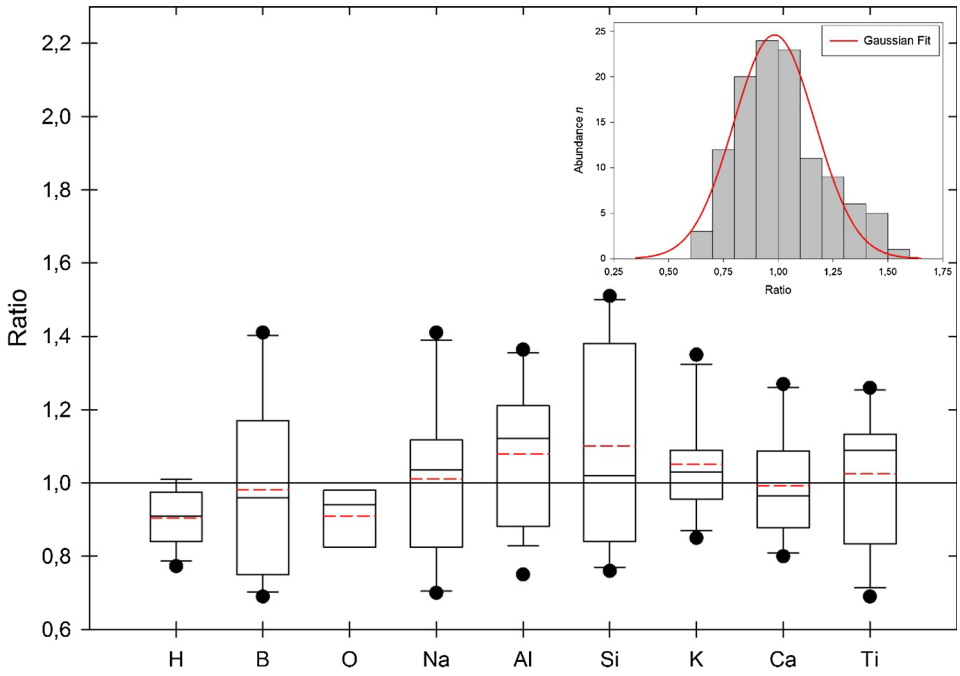

Fig. 5 *Box*-and-*whisker* plots of the ratios for each element and Gaussian distribution of all data. *Continuous and dashed lines* in the *boxes* represent the median and arithmetic mean, respectively. The *close symbols* represent the outliers

assay of 1860 s by LS-PGNAA (4 and 145 mg kg^{-1}) [27] due to a lower thermal neutron flux. Nevertheless the detection limits achieved are comparable to those estimated for a 2000 s assay of a concrete matrix in 8-gal drums with another PGNAA-system (9 and 115 mg kg^{-1} for cadmium and mercury and 4.4 g kg^{-1} for lead) [23]. As shown in Fig. 6 the detection limits increase smoothly with increasing polyethylene content of the sample. The increase of the detection limit for cadmium and mercury is mainly related to the product of the gamma-ray detection efficiency [28] and the thermal neutron flux (Table 2), the background below the considered gamma-rays being nearly the same for all samples due to the high prompt gamma background activity of the facility. In the case of lead the increase of the detection limit is essentially caused by the decrease of the fast neutron flux.

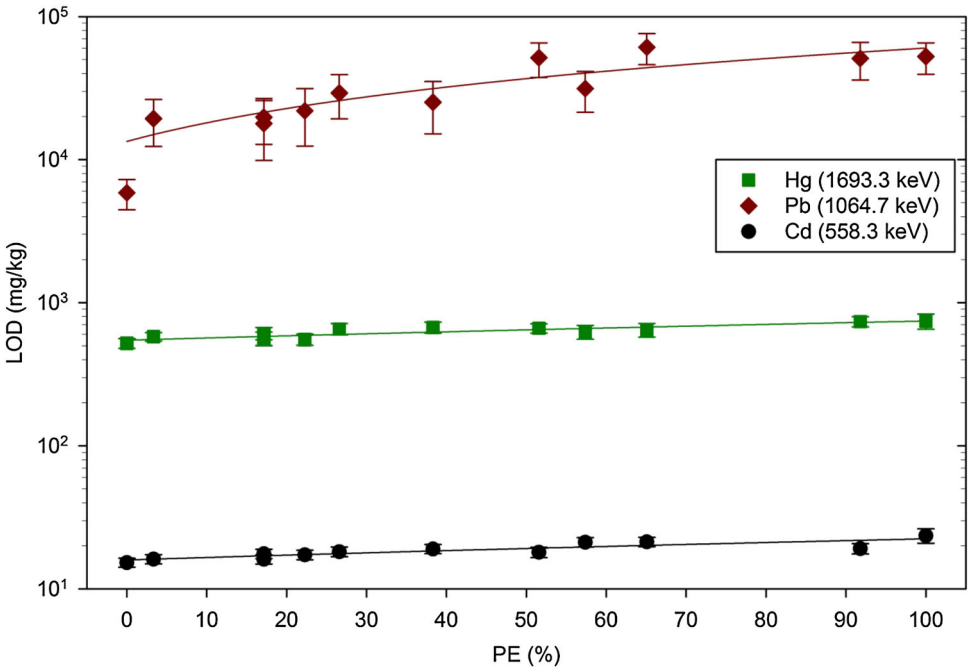

Fig. 6 Detection limits for cadmium, mercury and lead as a function of the polyethylene content of the samples

Conclusion

In this study LS-CNAA of 200 L steel drums filled with concrete and polyethylene was performed with a pulsed 14 MeV neutron source recording successively prompt and delayed gamma-ray spectra between the neutron pulses. Thermal neutron die-away times were measured to correct prompt gamma background interferences and to determine the thermal neutron flux in neutron pulses. We showed that the fast neutron flux may be estimated from the results obtained by thermal neutron capture with some assumptions on the sample composition according to the detected delayed gamma rays. The method proposed to evaluate the sample composition provides for the homogeneous samples a good agreement between measured and expected values within uncertainties. For the heterogeneous samples the determined elemental contents agree with the expected values within ±39%; the large deviations observed being mainly associated to local perturbations of the fast and thermal neutron flux owing different neutron moderation and absorption properties of the materials. Possible techniques to improve results accuracy for heterogeneous samples are proposed in [28]. Improvement of counting statistics and detection limits as well as a reduction of background interferences may be achieved through a better neutron/gamma shielding of the HPGe-detector [41]. Additionally a higher detection sensitivity of the fast neutron activation products may be achieved through an optimization of the length and repetition period of the fast neutron pulses relative to their half-lives.

References

1. Bode P, Overwater RMW (1993) Trace-element determinations in very large samples: a new challenge for neutron activation analysis. J Radioanal Nucl Chem 167:169–176
2. Overwater RMW, Bode P, de Goeij JJM, Hoogenboom JE (1996) Feasibility of elemental analysis of kilogram-size samples by instrumental neutron activation analysis. Anal Chem 68:341–348
3. Blaauw M, Lakmaker O, van Aller P (1997) The accuracy of instrumental neutron activation analysis of kilogram-size inhomogeneous samples. Anal Chem 69:2247–2250
4. Bode P, Overwater RMW, de Goeij JJM (1997) Large-sample neutron activation analysis: present status and prospects. J Radioanal Nucl Chem 216:5–11
5. Baas HW, Blaauw M, Bode P, de Goej JJM (1999) Collimated scanning towards 3D-INAA of inhomogeneous large samples. Fresenius J Anal Chem 363:753–759
6. Blaauw M, Baas HW, Donze M (2003) Height-resolved large-sample INAA of a 1 m long, 13 cm diameter ditch-bottom sample. Nucl Instrum Methods Phys Res A 505:512–516
7. Lin X, Henkelmann R (2002) Instrumental neutron activation analysis of large samples: a pilot experiment. J Radioanal Nucl Chem 251:197–204
8. Vasilopoulou T, Tzika F, Koster-Ammerlaam MJJ, Stamatelatos IE (2011) Large sample neutron activation analysis of a reference inhomogeneous sample. J Radioanal Nucl Chem 289:731–737
9. Haddad Kh, Alsomel N (2011) Large sample neutron activation analysis of municipal solid waste using shutdown MNSR photoneutrons. J Radioanal Nucl Chem 288:823–828
10. Vasilopoulou T, Tzika F, Stamatelatos IE (2012) Collimated scanning for large sample neutron activation analysis of inhomogeneous samples. J Radioanal Nucl Chem 291:479–483
11. Stamatelatos IE, Tzika F, Vasilopoulou T, Koster-Ammerlaam MJJ (2010) Large sample neutron activation analysis of a ceramic vase. J Radioanal Nucl Chem 283:735–740
12. Vasilopoulou T, Stamatelatos IE, Montoy EH, Bedregal PS, Tsalafoutas I, Bode P (2015) Large sample neutron activation analysis of irregular-shaped pottery artifact. J Radioanal Nucl Chem 303:853–858
13. Tzika F, Stamatelatos IE, Kalef-Ezra J, Bode P (2004) Large sample neutron activation analysis: correction for neutron and gamma attenuation. Nukleonika 49(3):115–121
14. Zhang HQ, Ni BF, Tian WZ, Zhang GY, Huang DH, Liu CX, Xiao CJ, Sun HC (2011) Correction factors for the gamma attenuation effects in large sample neutron activation analysis. J Radioanal Nucl Chem 287:513–517
15. Mandour MAA, Badawi A, Mohamed NMA, Emam A (2016) Towards a methodology for bulk sample neutron activation analysis. J Taibah Univ Sci 10:235–241
16. Overwater RMW, Bode P (1998) Computer simulations of the effects of inhomogeneities on the accuracy of large sample INAA. Appl Radiat Isot 49:967–978
17. Sueki K, Kobayashi K, Sato W, Nakahara H, Tomizawa T (1996) Nondestructive determination of major elements in a large sample by prompt gamma ray neutron activation analysis. Anal Chem 68:2203–2209
18. Degenaar LH, Blaauw M, Bode P, de Goeij JJM (2004) Validation of MCNP for large sample thermal-beam prompt-gamma neutron activation analysis. J Radioanal Nucl Chem 2:311–315
19. Blaauw M, Degenaar LH, de Goeij JJM (2007) Development of a non-invasive method for the determination of the macroscopic neutron cross sections of a sample matrix in large-sample prompt-gamma neutron activation analysis. J Radioanal Nucl Chem 3:765–770
20. Blaauw M, Belgya T (2005) Neutron self-shielding correction for prompt gamma neutron activation analysis of large samples. J Radioanal Nucl Chem 265:257–259
21. Whetstone ZD, Kearfott KJ (2014) A review of conventional explosives detection using active neutron interrogation. J Radioanal Nucl Chem 301:629–639
22. Lim CA (2004) Recent development in neutron-induced gamma activation for on-line multielemental analysis in industry. J Radioanal Nucl Chem 262:525–532
23. Dulloo AR, Ruddy FH, Congedo TV, Gehrke RJ (1998) Detection limits of a laboratory pulsed gamma neutron activation analysis system for the nondestructive assay of mercury, cadmium and lead. Nucl Tech 123:103–112
24. Mauerhofer E, Havenith A (2014) The MEDINA facility for the assay of chemotoxic inventory of radioactive waste packages. J Radioanal Nucl Chem 302:483–488
25. Randriamalala TH, Rossbach M, Mauerhofer E, Zs Révay, Söllradl S, Wagner FM (2016) FaNGaS: a new instrument for (n, n′γ) reaction measurements at FRM II. Nucl Instrum Methods Phys Res A 806:370–377
26. Rossbach M, Randriamalala T, Mauerhofer E, Zs Révay, Söllradl S (2016) Prompt and delayed inelastic scattering reactions from fission neutron irradiation—first results of FaNGaS. J Radioanal Nucl Chem 309:149–154

27. Mauerhofer E, Havenith A, Kettler (2016) Prompt gamma neutron activation analysis of a 200 L steel drum homogeneously filled with concrete. J Radioanal Nucl Chem 309:273–278
28. Mildenberger F, Mauerhofer E (2016) Prompt gamma neutron activation analysis of large heterogeneous samples composed of concrete and polyethylene. J Radioanal Nucl Chem 309:1265–1269
29. Mildenberger F, Mauerhofer E (2016) Thermal neutron die-away times in large samples irradiated with a pulsed 14 MeV neutron source. J Radioanal Nucl Chem 307:661–667
30. Molnár GL (2004) Handbook of prompt gamma activation analysis with neutron beams. Kluwer Academic Publishers, Berlin
31. Database of prompt gamma rays from slow neutron capture for elemental analysis, IAEA library cataloguing in publication data, ISBN 92-0-101306-X, Vienna January 2007
32. Havenith A (2015) Stoffliche Charakterisierung radioaktiver Abfallprodukte durch ein Multi-Element-Analyseverfahren basierend auf der instrumentellen Neutronen-Aktivierungs-Analyse—MEDINA—Schriften des Forschungszentrum Jülich, Energie & Umwelt/Energy & Environment, Band/Volume 248, ISBN 978-3-95806-033-2
33. Givens WW, Mills WR, Caldwell RL (1970) Cyclic activation analysis. Nucl Instrum Methods 80:95–103
34. Chadwick MB, Herman M, Oblozinsky P et al (2011) ENDF/B-VII.1 nuclear data for science and technology: cross sections, covariances, fission product yields and decay data. Nucl Data Sheets 112(12):2887–2996
35. Erdtmann G (1976) Neutron activation tables, vol 6., Kernchemie in EinzeldarstellungenVerlag Chemie, New York
36. Chu SYF, Ekström LP, Firestone R, The Lund/LNBL Nuclear Data Search, Version 2.0, February 1999. http://nucleardata.nuclear.lu.se/toi/
37. Kettler J (2010) Prompt-Gamma-Neutronen-Aktivierungs-Analyse zur zerstörungsfreien Charakterisierung radioaktiver Abfälle, Schriften des Forschungszentrum Jülich, Energie & Umwelt/Energy & Environment, Band/Volume 82, ISBN 978-3-89336-665-1
38. Tables of cross sections calculated from JENDL-4.0, Tables of Nuclear Data, Nuclear Data Center, Japan Atomic Energy Agency. http://wwwndc.jaea.go.jp/NuC/index.html
39. Shibata K, Iwamoto O, Nakagawa T, Iwamoto N, Ichihara A, Kunieda S, Chiba S, Furutaka K, Otuka N, Ohsawa T, Murata T, Matsunobu H, Zukeran A, Kamada S, Katakura J (2011) JENDL-4.0: a new library for nuclear science and engineering. J Nucl Sci Technol 48:1–30
40. Belgya T (2012) Prompt gamma activation analysis at the Budapest research reactor. Phys Proc 31:99–109
41. Nicol T, Mauerhofer E, Carasco C, Perot B, Collot J (2016) HPGe-detector shielding optimization with MCNP for the MEDINA neutron activation cell. J Radioanal Nucl Chem. doi:10.1007/s10967-016-4816-3